

Rapid fabrication of metal-coated composite stereolithography parts

Z Zhou^{1*}, D Li¹, J Zeng¹, and Z Zhang²

¹State Key Laboratory for Manufacturing Systems Engineering, Xi'an Jiaotong University, Xi'an, People's Republic of China

²China Aerodynamics Research and Development Center, Mianyang, People's Republic of China

The manuscript was received on 29 January 2007 and was accepted after revision for publication on 11 May 2007.

DOI: 10.1243/09544054JEM827

Abstract: In this paper, the rapid fabrication method based on stereolithography (SL) and electrochemical deposition is described in detail and mechanical test results of composite nickel-coated SL parts are presented. Coatings of electrodeposited nickel on SL prototypes result in increases in Young's modulus, UTS, flexural modulus, and strength. Electrodeposited nickel coating has dramatically improved the overall strength and stiffness of SL parts. The adhesive strength of the roughened SL resin–nickel interface is higher than the original. In particular, the influence of the surface roughness on adhesive strength between SL and metal is investigated. Moreover, this paper has presented an application of a structural electrodeposited nickel coating over SL parts to make a functional airfoil model with a complex internal structure and sufficient mechanical strength and stiffness.

Keywords: stereolithography, electrochemical deposit, composite, rapid prototyping and manufacturing (RP&M)

1 INTRODUCTION

Rapid prototyping and manufacturing (RP&M) represents a group of novel manufacturing methods widely used in engineering for the quick fabrication of geometrically complex conceptual and functional solid models [1–3]. The stereolithography (SL) process has always been one of the most significant RP technologies and it is one of the technologies that is considered to be suitable as a future end-use part manufacturing process [4]. However, full functional prototypes with the full range of a part's properties cannot be built with SL because of the limited material properties of epoxy resins. SL models have limited functionality owing to low strength and stiffness, poor creep performance, and environmental instability (moisture and temperature) [5, 6].

Many methods can be used to reinforce epoxy resin and SL models, among which coating with copper or nickel on the surface of the SL models shows promise [7–9]. The application of a protective

electroplated coating can add strength and rigidity to parts and also reduce any effects of ageing caused by absorption of water or ultraviolet light; however, it may adversely affect feature resolution and tolerance. If the reinforcing coating is very thin and the electrodeposition process is within the limits of the model's stability, metal coating can improve the mechanical and physical properties without changes to a part's functional dimensions [10, 11]. The obvious advantage of SL models coated with metal is better mechanical performance, enabling the fabrication of composite SL parts with higher loading capability.

The purpose of this paper is to present an application of an electrodeposited nickel coating over SL parts to make composite parts with good mechanical performance. Experimental procedures are described in detail. SL part surfaces treated by chemical roughening are observed and the adhesive strength of the SL–metal composite interface is evaluated by tensile testing. Mechanical testing data are presented for the nickel-coated SL tensile and flex test samples with different coating thicknesses. This paper also presents a hybrid design and fabrication method for a metal-coated SL airfoil model with independently movable deflecting surfaces and internal passages.

*Corresponding author: State Key Laboratory for Manufacturing Systems Engineering, Xi'an Jiaotong University, Xi'an, Shangxi 710049, People's Republic of China. email: zzh_zhou@eyou.com

Finally, the numerical simulation method combining computational fluid dynamics (CFD) and finite element analysis (FEA) is applied to predict the maximum stress and deflection of the airfoil model in order to check the strength of the nickel-coated SL airfoil model under aerodynamic loads.

2 EXPERIMENTAL PROCEDURES

2.1 Production of stereolithography parts

In this research, SL was employed to fabricate the resin prototype of test samples and models. The SL apparatus SPS 600B was developed by The Institute of Advanced Manufacturing Technology (IAMT) at Xi'an Jiaotong University. The computer aided design (CAD) models were converted into STL data and then sliced into 0.05 mm layer thickness in data-processing software (RP-Data, IAMT). The resin prototypes could then be fabricated quickly and automatically using Somos 14120 resin from the DSM Corporation. Thorough washing of the parts in acetone solvent was required to remove excess resin. After the removal of excess resin, the SL parts were completed by manual finishing and post-curing using a UV light box for 30 min.

2.2 Surface roughening

The adhesion between electrodeposited metal coating and the untreated SL part is typically poor owing to the original smooth surface of the SL part. To achieve a sufficient adhesion of deposited metal on SL resin, chemical treatment was used to roughen the SL part surface because of its simplicity and low cost. After being degreased and cleaned in alkaline solution (magnesia 50 g/l, sodium phosphate 10 g/l) for 10 min, the SL parts were immersed in chrome acid solution (chromium trioxide 125 g/l, sulfuric acid 200 ml/l, nitric acid 210 ml/l) for 30 min for roughening treatment, and then immersed in permanganate solution (potassium permanganate 20 g/l, potassium hypochlorite 100 g/l) for 20 min to obtain a uniform microroughness on the SL part surface. Subsequently, the SL parts were immersed in 10 per cent hydrochloric acid for 5 min to complete smear removal of the manganese dioxide precipitation and the SL parts had to be rinsed simply with distilled water after each step.

2.3 Electroless nickel deposition

Prior to the electrodepositing process, the SL part surface must be made conductive. This can be done through electroless deposition or by the use of conductive additives such as carbon. For this work, electroless deposition is chosen because it provides a

better bond than carbon painting. Therefore, electroless deposition was done with a sequence of preparatory steps in a room temperature electroless nickel bath, which deposited a 1–2 μm thick layer of nickel to make the surfaces conductive. Firstly, the SL parts were placed in an acidic stannous chloride solution (stannous chloride 10 g/l, hydrochloric acid 40 ml/l) for 10 min, then rapidly into a formaldehyde solution (10 per cent) after activation in a solution of palladium chloride (palladium chloride 1 g/l, hydrochloric acid 10 ml/l) at room temperature; palladium was reduced to its catalytic metallic state by the tin. Thus the treated parts were deposited with nickel from an electroless nickel solution consisting of nickel sulphate (20 g/l), sodium citrate (10 g/l), sodium hypophosphite (30 g/l), and ammonium chloride (30 g/l). Consequently, the thin metal-foil layer formed a conductive surface and then the parts were sent to the next operation for electrodeposition with nickel.

2.4 Nickel electrodeposition

Electrodeposition has been identified as a feasible and economical technique for industrial application such as electronics and jewellery manufacture. In this work, the advantage of employing a high metal content (nickel sulphate 250 g/l, nickel chloride 50 g/l) was that a higher current density (4–5 A/dm²) can be used and a thicker deposit (0.5 mm) can be produced in a reasonable time. Boric acid (35 g/l) was used as a buffer to maintain the bath pH, sodium lauryl sulphate (0.015 g/l) and 2-butyne-1,4-diol (0.25 g/l) as wetting agents to reduce the risk of pitting, and saccharin (1 g/l) as an inhibitor to reduce grain size of the deposit. The pH was adjusted to a constant value of 4.5 ± 0.1 by adding nickel chloride to raise it or a hydrochloric-sulfuric acid mixture (1:7) to lower it. A thermostatic heater and gas agitator were used in the electrolyte bath kept at a constant temperature of 40 ± 1 °C.

Figure 1 shows some nickel-coated SL parts made by the above processes. The holes on the part shown in Fig. 1(a) and the complex structure of the aircraft model shown in Fig. 1(b) indicate the high degree of surface detail that may be maintained when SL parts are electrodeposited.

2.5 Test procedures and samples

Surface morphology and the roughening effect of SL resin samples were studied by optical microscope (Keyence VH-8000). The thickness of nickel coating was measured using the optical microscope. For each specimen, five readings for thicknesses of different cross-sections were taken at positions that were not close to any edges. The metal thickness reported for the tests is based upon the average of the five

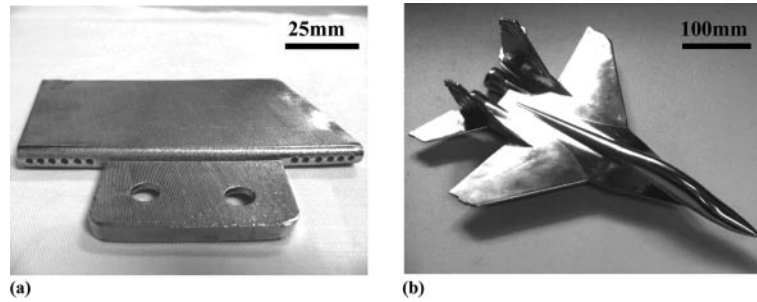


Fig. 1 Electrodeposited SL parts with nickel coating: (a) electrodeposited SL part with holes; (b) nickel-coated SL model with complex structure

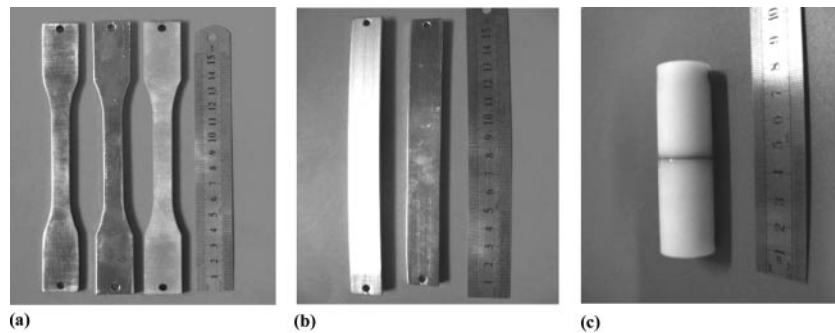


Fig. 2 Mechanical test samples: (a) tensile test samples; (b) flex test samples; (c) adhesion strength test sample

readings in the test section of the specimens after coating.

The mechanical tests in this work included tensile, flexural, and adhesive strength tests between SL resin and nickel coating. The tests were conducted strictly according to ISO standards [12–14]. Tensile testing was carried out following ISO-527 while flexure testing was carried out following ISO-178 using a span to depth ratio of 32:1. The adhesive strength of the coatings was measured according to the ISO-2819 standard. The tensile, flexural, and adhesive strength test samples were fabricated from Somos 14120 resin. Therefore, the nickel coatings were deposited over the sample surfaces of the tensile and flexural tests (Figs 2(a) and (b)). Each specimen of the adhesive strength test was electrodeposited on the end face, and its face was bonded to the same-diameter bar end by the commercially available epoxy resin XD 911 adhesive (Fig. 1(c)). Three specimens at each metal coating thickness are provided for the evaluation of mechanical properties by an Instron type testing machine.

3 RESULTS AND DISCUSSION

3.1 Roughening effect

The SL original and roughened surfaces as seen by the optical microscope (Keyence VH-8000) are shown

in Figs 3(a) and (b) respectively. Chemical roughening of the SL surface was effected by oxidation with potassium permanganate/potassium hypochlorite and chromic/sulphuric acids that were in practice applied exclusively as the media for oxidation treatment. With chemical roughening treatment, small voids and pores materialized and the surface looked porous as depicted in Fig. 3(b). This suggested that some components of SL resin could be degraded under chemical treatment. Therefore, the electrodeposited nickel filled the holes caused by roughening and anchored itself mechanically in the SL resin surface. Moreover, during activation metal nuclei were adsorbed on the walls of the pores and cavities and nickel particles at first covered the pores and cavities and then gradually the entire surface. The interlocking sites are clearly visible from the light micrographs as depicted in Fig. 3(c). Consequently, the thin metal-foil layer formed a conductive surface and then the parts were sent to the next operation for electrodeposition with nickel as depicted in Fig. 3(d).

A number of publications [15, 16] exist on surface treatments for improving the adhesion strength of copper on epoxy resins. Sam and Alfons [17] study the effect of wet chemical pretreatments on the interfacial adhesion between plated copper layers and epoxy polymers. These authors have made a phenomenological study of copper-laminated foils and

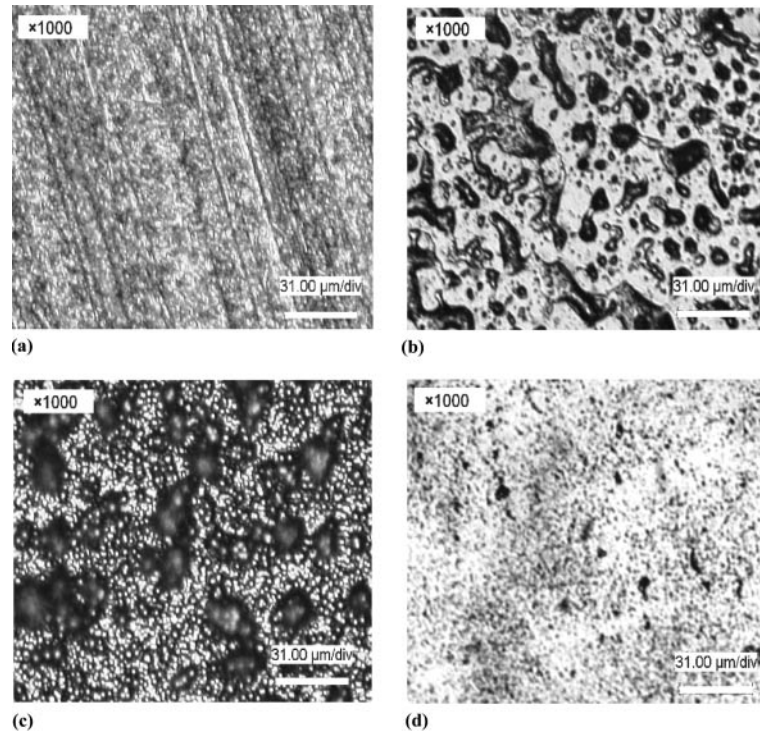


Fig. 3 Optical micrographs of uncoated and nickel-coated SL surface before and after chemical roughening: (a) original SL surface; (b) roughened SL surface; (c) electroless deposited nickel surface; (d) electrodeposited nickel surface

divided the mechanisms of adhesion into three groups:

- (a) mechanical interlocking;
- (b) physical bonding;
- (c) chemical bonding.

These studies have demonstrated by various methods that chemical bonds between metal and SL are not an essential contributory factor for adhesive strength. Chemical adhesive forces between metal coating and SL resin surface are of minor importance.

The observed influence of the SL substrate surface roughness on the adhesion strength favours the assumption that mechanical interlocking, created by the chemical roughening, is the most important factor in determining the adhesion mechanism of the nickel coatings electrodeposited at room temperature on SL substrates; that is, the adhesion can be explained by mechanical anchoring of the metal coating on the SL surface. Consequently, for the metal coating by the conventional electrodeposition processes, it is believed that the mechanical interlocking effect is the main bonding mechanism at the substrate-coating interface rather than the chemical bonding. Therefore, the pores and cavities caused by chemical roughening can increase the adhesive area and improve the mechanical interlocking effect between the metal deposit and the SL surface. The adhesive strength between the substrate and metal

coating can be enhanced with an increase of the substrate surface roughness. Therefore, it is quite possible to adopt chemical roughening to optimize the bonding performance of the SL substrate with nickel coating.

3.2 Adhesive strength

Figure 4(a) shows the typical stress-strain curve of fracture behaviours in tensile tests for the deposited nickel/SL interface. Furthermore, the results of adhesive strength between the nickel coating and the SL substrate with original and roughened interfaces are shown in Fig. 4(b) with respect to coating thickness. The adhesive strength at 0.05 mm becomes the lowest, 2.6 MPa and 5.7 MPa for the original and roughened SL samples respectively. Figure 4(b) also shows that the adhesive strength maximum is 5.3 MPa at the 0.15 mm coating thickness for the original untreated SL parts. Nevertheless, the adhesive strength attains a maximum value 11.1 MPa at the coating thickness of 0.25 mm for the roughened SL parts. The variation of the adhesive strength before and after chemical roughening also indicates that the enhanced adhesion strength can be obtained by the optimized careful chemical roughening process of the SL substrate surface before the coating deposition.

However, after chemical roughening, it is found that the adhesive strength decreases when the coating

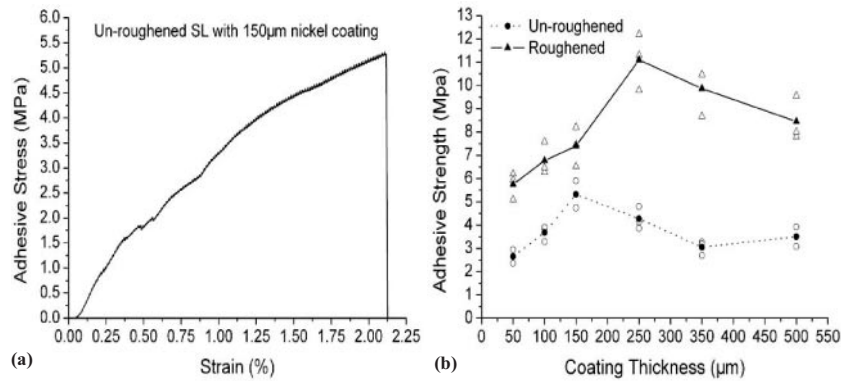


Fig. 4 Typical stress–strain curve and experimental values of adhesive strength by tensile test: (a) typical stress–strain curve for adhesive strength test; (b) adhesive strength with different coating thickness

thickness increases from 0.25 mm to 0.5 mm. A possible cause leading to the phenomenon may be the accumulation of residual stress during electro-deposition. This implies that the adhesive strength of deposited coatings will be influenced by the electro-deposition process conditions in addition to the surface roughness of the SL substance. Moreover, the present experimental results evidently suggest that there is a limitation to the contribution of the mechanical bonding effect to the adhesion of electro-deposited coating and it can be found that most coatings presented achieved an adhesive strength in the range 2–12 MPa.

In other words, although the surface appears to be very rough after chemical roughening, the adhesion of the metal coating interface is, however, quite poor. A significant number of publications [17, 18] focus on the influence of the plating bath composition on the properties of the electroless deposited copper and report changes in adhesion owing to the plating bath composition. However, the influence of the substrate surface on which the electroless copper is plated on the adhesion strength is not very clear in these cases. Surface modification for the adhesion improvement of electroless copper has been researched for imides, ceramic materials, and liquid crystalline polymers [18, 19] and image analysis of the fracture surface upon tensile testing is proven to be an excellent tool for determining the extent of the adhesive and cohesive failures [20].

For this work, Fig. 5 shows the typical light micrographs of the back side of the coating nickel and the corresponding SL substrate surface after decohesion. The fracture occurred at the interface of electrodeposited nickel coating and electroless deposited nickel foil, which was directly associated with the adhesive strength between SL and coating. Consequently, the adhesion between the electroless deposited nickel foil and the SL substrate is greater than between the

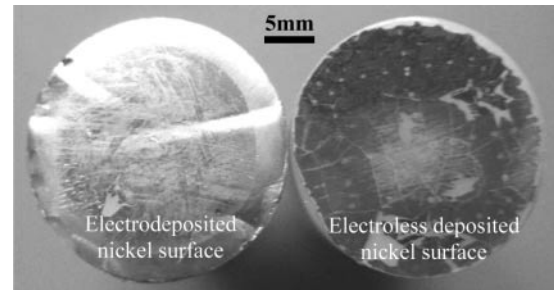


Fig. 5 Optical micrographs of typical fracture surface from adhesive strength test

electrodeposited nickel coating and the electroless deposited nickel foil. Moreover, the adhesive strength is qualitatively determined by the fracture mechanism that tests the ability of an interface to resist the propagation of a crack. However, this also indicates that the adhesion between the electrodeposited nickel coating and the electroless deposited nickel foil is not strong enough to resist the higher decohesion loads as depicted in Fig. 5. Therefore, some treatment methods should be used to improve the adhesion of the interface between the electrodeposited nickel coating and the electroless deposited nickel foil and further research is needed.

In addition, an optimum microstructure of pores and cavities in the roughened SL substrate will ensure good adhesion because the mechanical interlocking is the most important factor determining the adhesion mechanism. These optimum pores and cavitations serve as interlocking sites, thus the adhesive strength to metal coating will be increased sharply. Furthermore, adhesive strength improvements can be achieved through the chemical roughening treatment method. However, there is a limited contribution to the bonding effect or adhesive strength for the chemical roughening treatment. This means that

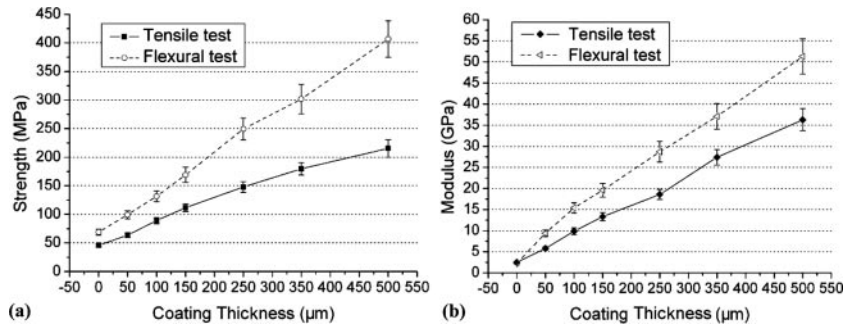


Fig. 6 Tensile and flexural test results of the nickel-coated samples with different coating thickness: (a) ultimate tensile and flexural strength; (b) Young's and flexural modulus

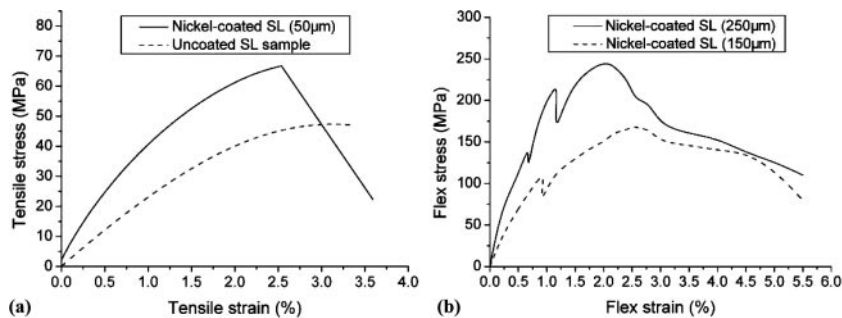


Fig. 7 Typical stress–strain curves from tensile and flex tests of nickel-coated SL samples: (a) stress–strain curve from tensile test; (b) stress–strain curve from flex test

it is important to improve the interface adhesion by other treatment methods in order to obtain fully functional metal–SL composite parts used under loading conditions.

3.3 Tensile and flexural test results

Metal-coated SL polymer has the properties of a bonded composite material. The hard and stiff metal coating, firmly anchored in the SL material, confers new mechanical properties on the material that differ from those of the individual components. The result of the tests depends on the thickness of the metal coat as depicted in Fig. 6. A simultaneous increase in tensile and flexural strength is typical for the reinforced SL materials with nickel coating.

Figures 6(a) and (b) show the measured strength and modulus values for the coated SL test parts respectively. As expected, the ultimate tensile strength (UTS) of a nickel-coated SL sample is greater than that of the uncoated counter samples, being increased usually by a factor of between 2 and 6, the actual gain in strength depending on the ratios of the combined thickness and tensile strength of the metal coating to those of the SL resin substrate. The flexural modulus or stiffness of the plated SL parts is much increased, being approximately 4–20 times greater than that of unplated counter SL parts; that is, the origin of

mechanical properties comes from the fact that parts are composed of hybrid materials (resin and metal). Even if the metal thickness is thin, 0.05 mm, it completely modifies the behaviour of parts. Again, thicker coatings lead to higher mechanical properties as would be expected and there appears to be an increase of the trend lines as the coating thickness of the metal increases.

Figure 7(a) gives the tensile stress–strain curves of SL samples with and without 0.05 mm nickel coating respectively. Compared with the uncoated SL sample, the nickel-coated SL sample tested in tensile conditions shows a more pronounced increase in UTS with increasing strain. The coating of a thin layer of nickel has changed the tensile characteristics of the SL resin. Furthermore, fracture is not observed at a 2.5 per cent tensile strain for the uncoated SL samples and the strain at break is 3.5 per cent. In contrast, the tensile stress–strain curve for the nickel-coated specimens showed a much steeper slope, and fracture was observed at the same strain of 2.5 per cent with a higher load. As can be seen in the figure, this nickel-coated SL sample exhibits a little lower strain at break than the uncoated counter sample and the fracture behaviour of the nickel-coated SL sample shows as brittle.

The flexural stress–strain curves of SL samples with 0.15 mm and 0.25 mm nickel coating are shown in

Fig. 7(b). The SL samples with 0.25 mm nickel coating are about 1.5 times stiffer and stronger than with 0.15 mm coating without a significant reduction in the strain to failure. Moreover, the flexural strain at failure for nearly all the samples hovers near 2 per cent through all the coating levels studied and there is a slight decline in some samples at the thinner coating. Moreover, the stress–strain curves from the metal-coated SL flexural test (Fig. 7(b)) are typical for any mechanical stress caused by tension, bending, torsion, and impact: when a firm bond exists between metal and resin, the stresses are first taken up by the considerably stiffer metal. Deformation is elastic and reversible, as long as the expansion remains within the cross-section under stress. However, the breaking limit is exceeded owing to the extremely high stress concentration and notch effect. When the metal fractures, the resin will also invariably break. Therefore, it is important to improve the adhesion interface between the SL resin and metal coating in order to obtain functional metal–SL parts used under loading conditions.

The flexure modulus and strength values rise more sharply with increased metal thickness than the Young's modulus and UTS values respectively. This may be due to the fact that the influence of the adhesive interface for the flexural test is more than for the tensile test and the moment of area is important for flexural tests. This means that, except for the adhesive strength between SL and coating, the effect of geometrical factors of the tensile and flexural specimens is also important. Moreover, the geometrical factors of flexural samples are different from those of tensile samples in this work. Furthermore, for a given substrate thickness, the thicker the coating layer, the greater is the strengthening and stiffening effect. If the thickness of the coating is fixed, then the overall strengthening and stiffening effect will decrease with increasing SL substrate thickness. Therefore, the strengthening and stiffening effect will be more significant for the thin cross-section SL substrate than for thick cross-section ones.

4 APPLICATION: RAPID FABRICATION OF COMPOSITE WIND TUNNEL MODEL

Rapid prototyping (RP) allows the fabrication of complex three-dimensional structures. This has made it easier to incorporate surface pressure taps and passages into the airfoil wind-tunnel model. Furthermore, RP permits the one-step fabrication of a complex wind-tunnel model with internal passages and exterior contours [21]. This greatly reduces machining costs and time. However, RP models built entirely with plastics and resins are generally not stiff or strong enough to withstand the loads in a

wind-tunnel test [22]. In the application, strength and stiffness are added to the model by using an electrolytic metal coating over SL components of the airfoil model. The non-metallic SL parts are then reinforced by metal coating to form a hybrid airfoil model with internal passages and movable deflecting surfaces.

4.1 Design of wind tunnel model

The CAD wind tunnel model of an entire aircraft with airfoil, fuselage, and empennage is shown in Fig. 8(a). The airfoil is one of the main parts or components to withstand the loads in wind-tunnel testing. In order to fabricate the airfoil model and take into consideration the thickness of the applied coating, it is necessary to offset the airfoil CAD model surfaces inwards by the coating thickness. Therefore, the authors offset all of the airfoil model's features inwards by 0.1 mm thickness in the CATIA software (Dassault, France) as shown in Fig. 8(b).

One of the design goals is to provide three pairs of independently movable deflecting elevons and foreflaps that can be positioned at $0 \pm 20^\circ$ in the airfoil model. Therefore, the model was broken into four pieces: main airfoil, two pairs of different elevons at the trailing edge, and one pair of flaps at the leading edge as depicted in Fig. 8(c). In addition, the 8 mm diameter fixing pins were also incorporated into the airfoil model to align and fasten the components during assembly. The pin holes were designed with the length range of 3–10 mm in different surface locations.

Another design goal is to add 24 pressure taps and passages to the airfoil model in order to measure the surface pressure. Therefore, the pressure taps on the airfoil were designed and located at 10 per cent, 40 per cent, 60 per cent, and 80 per cent of the chord and were perpendicular to the exterior surface of the airfoil model as depicted in Fig. 8(d). The diameter of each tap and passageway was 0.8 mm. The bend radius closest to the pressure tap location was a minimum of 1.40 mm and all of the other bend radii were at least 3.50 mm. These bend radii should be increased as soon as space permits to reduce pressure equilibrium time.

4.2 Manufacturing and assembly

The SL prototype components of the airfoil model were fabricated on SL apparatus, SPS 600B, and roughened by chemical treatments as depicted in Fig. 9(a). Next, a thin nickel-foil layer formed a conductive surface on SL prototypes by the electroless nickel deposition process (Fig. 9(b)). Therefore, the nickel-coated SL components of the airfoil model

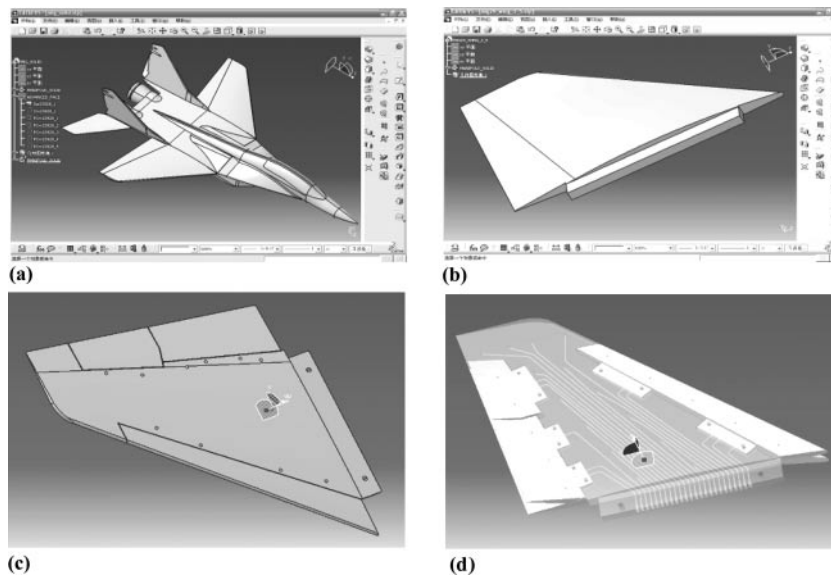


Fig. 8 Modification and redesign process of the airfoil pressure wind-tunnel model: (a) aircraft CAD model; (b) airfoil model after offsetting; (c) airfoil model after segmentation; (d) pressure model after redesign

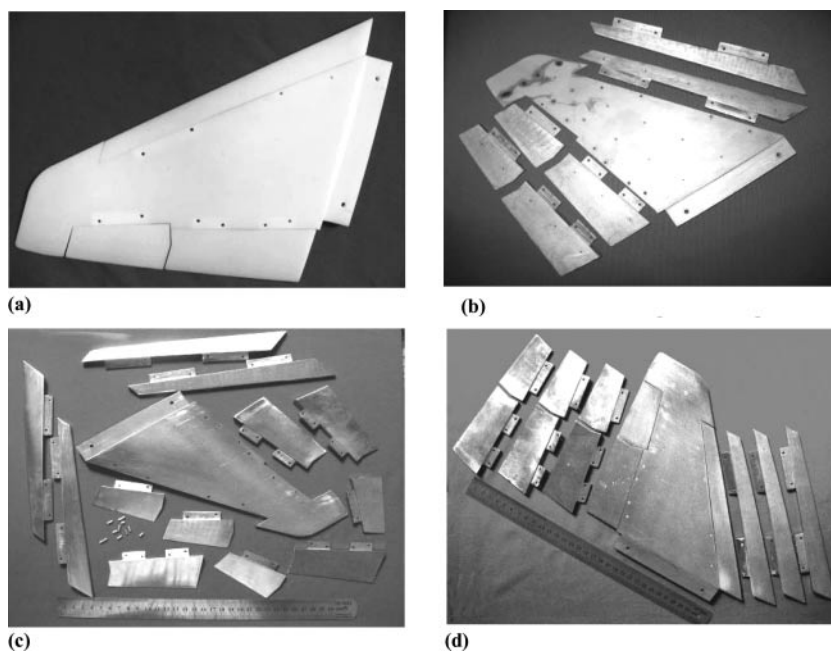


Fig. 9 Airfoil wind-tunnel components and model with deflecting elevons, foreflaps, and internal passages: (a) SL components of airfoil model; (b) electroless nickel deposited components; (c) nickel electrodeposited airfoil components; (d) airfoil model assembled with flaps

were created by the electrodeposition technique (Fig. 9(c)).

Final assembly of the components was performed using the fixing pin and rectangular plate. The metal-coated flaps were attached to the main airfoil model by placing the fins and rectangular metal-coated plates into mounting holes and pockets in the main airfoil as depicted in Fig. 9(d). Any slight discontinuities in the airfoil surface between flaps

and main airfoil model were carefully blended and smoothed. After assembling, the composite nickel-coated SL airfoil model was obtained.

4.3 Mechanical properties prediction

For this work, given the extremely thin airfoil cross-sections in the current design, there was concern that the airfoil might fail or deflect excessively during

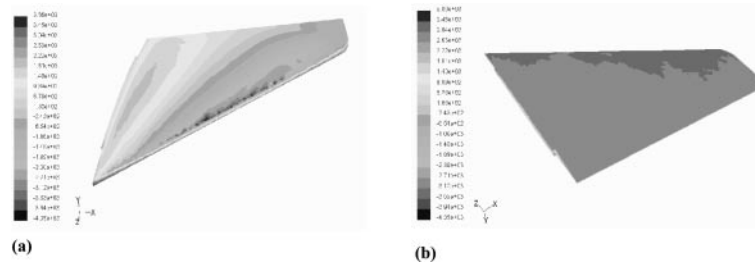


Fig. 10 Surface pressure contours of the airfoil model at 0.2 Ma, 20° angle of attack: (a) top surface pressure loads of airfoil model; (b) bottom surface pressure loads of airfoil model

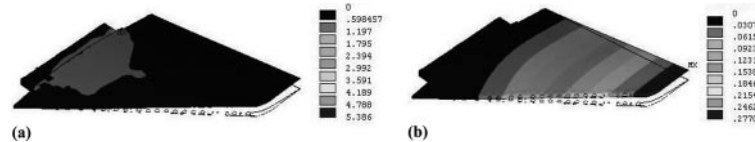


Fig. 11 Stress and deflection contours of the nickel-coated airfoil model: (a) airfoil stress contour at 0.2 Ma, 20° angle of attack; (b) airfoil deflection contour at 0.2 Ma, 20° angle of attack

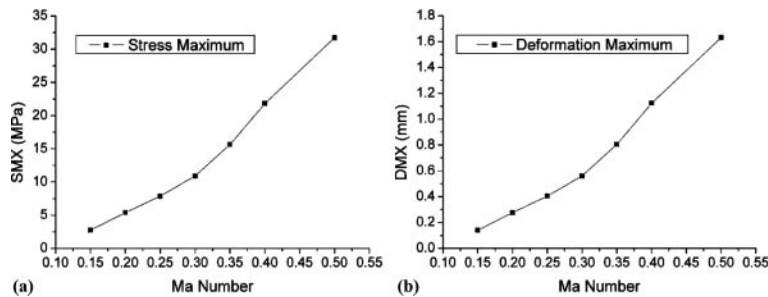


Fig. 12 Stress and deflection maximum of the nickel-coated airfoil model at a 20° angle of attack: (a) stress maximum in the range of 0.15–0.5 Ma; (b) deflection maximum in the range of 0.15–0.5 Ma

wind-tunnel testing, so an analysis was performed to estimate the stress and deflection for the metal-coated SL model configurations. CFD simulations were performed and used for calculating the airfoil loads. The predictions consisted of pressure values for the top and bottom airfoil surfaces. Once the applied pressure values and forces were known, an FEA was conducted on the airfoil model. These pressure data were then mapped onto the finite element model of the airfoil and the metal-coated airfoil was constrained where the fuselage was attached.

The analysis was run in ANSYS 10.0 (Ansys Corporation, USA) and the resulting pressure contours at the top and bottom surfaces of the airfoil are shown in Figs 10(a) and (b) respectively. The maximum predicted von Mises stress occurs on the top surface of the nickel-coated airfoil (Fig. 11(a)). The stress maximum, 5.38 MPa, is less than the allowable stress 44.8 MPa of the 0.1 mm nickel-coated SL material when the required factor of safety is 2.0 in subsonic wind-tunnel testing [23]. The maximum deflection at the airfoil tip is about 0.27 mm, as can be seen in the deflection contours shown in Fig. 11(b).

Stress and deflection results of the nickel-coated SL model in the range of 0.15–0.5 Ma at a 20° angle of attack are shown in Figs 12(a) and (b) respectively. The stress maximum increases rapidly from 2.73 MPa to 31.72 MPa and the deflection maximum increases from 0.14 mm to 1.63 mm. The allowable stress 44.8 MPa of the hybrid 0.10 mm nickel-coated SL material is more than 32 MPa which is the stress maximum at Ma 0.5. Consequently, the nickel-coated airfoil model is safe in the subsonic range, 0.15–0.5 Ma.

5 CONCLUSIONS

In the paper the mechanical test results of nickel-coated SL samples are presented: coatings of electro-deposited nickel on SL prototypes result in increases in Young's modulus, UTS, flexural modulus, and strength. In particular, the influence of the SL substrate roughness on adhesive strength between the SL and coating has been investigated and the adhesive strength of the roughened SL resin–nickel interface is higher than the original. These improvements allow

the fabrication of functional nickel-coated wind-tunnel models. The predicted results show that the strength of the nickel-coated airfoil model is sufficient in the subsonic range, 0.15–0.5 Ma. Furthermore, this method could potentially be used in fabricating other functional components or end-use parts with other RP techniques such as FDM, SLS, and LOM.

REFERENCES

- 1 **Chua, C. K., Leong, K. F., and Lim, C. S.** *Rapid prototyping: principles and applications*, 2003 (World Scientific, New Jersey).
- 2 **Quincieu, J., Robinson, C., Stucker, B., and Mosher, T.** Case study: selective laser sintering of the USUSat II small satellite structure. *Assembly Autumn*, 2005, **25**(4), 267–272.
- 3 **Wohlers, T.** Rapid prototyping and manufacturing-state of the industry report. *Annual worldwide progress report*, 2006 (Wohlers Associate Inc., USA).
- 4 **Cooper, K. G.** *Rapid prototyping technology: selection and application*, 2001 (Marcel Dekker Inc., New York).
- 5 **Dulieu-Barton, J. M. and Fulton, M. C.** Mechanical properties of a typical stereolithography resin. *J. Strain*, 2000, **36**(2), 81–87.
- 6 **Hague, R., Mansour, S., and Saleh, N.** Material and design considerations for rapid manufacturing. *Int. J. Prod. Res.*, 2004, **42**(22), 4691–4708.
- 7 **Hopkinson, N., Hague, R. J. M., and Dickens, P. M.** *Rapid manufacturing – an industrial revolution for the digital age*, 2006 (John Wiley & Sons, England).
- 8 **Saleh, N., Hopkinson, N., Hague, R. F. M., and Wise, S.** Effects of electroplating on the mechanical properties of stereolithography and laser sintered parts. *Rapid Prototyping J.*, 2004, **10**(5), 305–315.
- 9 **Griffiths, A.** Rapid manufacturing, the next industrial revolution. *J. Mater. World*, 2002, **10**(12), 34–35.
- 10 **Yarlagadda, P. K. D. V., Subramanian, V., and Christodoulou, P.** Feasibility studies on production of electro discharge machining electrodes by stereolithography and electroforming process. *J. Mater. Processing Technol.*, 1999, **89**, 231–237.
- 11 **Hague, R. J., Campbell, R. I., and Dickens, P. M.** Implications on design of rapid manufacturing. *Proc. Instn Mech. Engrs, Part C: J. Mechanical Engineering Science*, 2003, **217**, 25–30.
- 12 **ISO 527-1 and 2.** *Plastics – determination of tensile properties*, 1996.
- 13 **ISO 178.** *Plastics – determination of flexural properties*, 1997.
- 14 **ISO 2819.** *Electrodeposited and chemically deposited coatings – review of methods available for testing adhesion*, 1995.
- 15 **Christoph, J., Ebneith, H., Heymann, K., Meyer, M., Rempel, D., and Woldt, G.** *Electroplating of plastics – handbook of theory and practice*, 1977 (Hampton Hill, England).
- 16 **Ge, J., Turunen, M. P. K., and Kivilahti, J. K.** Surface modification and characterization of photodefinable epoxy/copper systems. *Thin Solid Films*, 2003, **440**, 198–207.
- 17 **Sam, S., Alfons, V., Etienne, S., and Andre, V. C.** Influence of chemical pretreatment of epoxy polymers on the adhesion strength of electrochemically deposited Cu for use in electronic interconnections. *J. Electrochem. Soc.*, 2004, **151**(2), 133–141.
- 18 **Jin, J. G., Lee, S. K., and Kim, Y. H.** Adhesion improvement of electroless plated Ni layer by ultrasonic agitation during zincating process. *Thin Solid Films*, 2004, **466**, 272–278.
- 19 **Charbonnier, M. and Romand, M.** Polymer pretreatments for enhanced adhesion of metals deposited by the electroless process. *Int. J. Adhes. Adhes.*, 2003, **23**(4), 277–285.
- 20 **Staia, M. H., Ramos, E., Carrasquero, A., Roman, A., Lesage, J., Chicot, D., and Mesmacque, G.** Effect of substrate roughness induced by grit blasting upon adhesion of WC–17% Co thermal sprayed coatings. *Thin Solid Films*, 2000, **377–378**, 657–664.
- 21 **Heyes, A. L. and Smith D. A. R.** Rapid technique for wind-tunnel model manufacture. *J. Aircr.*, 2004, **41**(2), 413–415.
- 22 **Springer, A.** Evaluating aerodynamic characteristics of wind-tunnel models produced by rapid prototyping methods. *J. Spacecraft Rockets*, 1998, **35**(6), 755–759.
- 23 **Qilin, Y.** *Wind tunnel testing handbook*, 2000 (National Defence Industry Press, Beijing, China).